# Photo double ionization of helium 100 eV and 450 eV above threshold: III. Gerade and ungerade amplitudes and their relative phases

**A Knapp[1], B Krässig[2], A Kheifets[3], I Bray[4], Th Weber[1,6,7],**
**A L Landers[5], S Schössler[1], T Jahnke[1], J Nickles[1], S Kammer[1],**
**O Jagutzki[1], L Ph H Schmidt[1], M Schöffler[1], T Osipov[6,7], M H Prior[7],**
**H Schmidt-Böcking[1], C L Cocke[6] and R Dörner[1]**

[1] Institut für Kernphysik, Universität Frankfurt, August-Euler-Str. 6, D-60486 Frankfurt, Germany
[2] Chemistry Division, Argonne National Laboratory, Argonne, IL 60439, USA
[3] Research School of Physical Sciences and Engineering, Australian National University Canberra ACT 0200, Australia
[4] Centre for Atomic, Molecular and Surface Physics, Murdoch University, Perth, 6150 Australia
[5] Physics Department, Auburn Univ., Auburn, AL 36849, USA
[6] Department of Physics, Kansas State University, Manhattan, KS 66506, USA
[7] Lawrence Berkeley National Laboratory, Berkeley, CA 94720, USA

E-mail: doerner@atom.uni-frankfurt.de

## Abstract

We present a joint experimental and theoretical study of the gerade and ungerade amplitudes of the photo double ionization of helium at excess energies of 100 eV and 450 eV above the threshold. We describe a method of extracting the amplitudes from a COLTRIMS data set. The experimental results are well reproduced by convergent close-coupling (CCC) calculations. The fully differential cross section data underlying this study can be found in our companion papers immediately preceding this one.

## 1. Introduction

Photo double ionization (PDI) in helium can be described by the fivefold differential cross section (5DCS) $d^5\sigma/(dE_1 d\Omega_1 d\Omega_2)$ with $d\Omega_i = \sin\Theta_i \, d\Theta_i \, d\Phi_i$. Here $\Theta_1$, $\Theta_2$ and $\Phi_1$, $\Phi_2$ are the polar and azimuthal emission angles of the electrons $e_1$ and $e_2$, respectively. $E_1$ is the energy of electron $e_1$. This fivefold differential cross section is often displayed in the form of an angular distribution of either the slow or the fast electron relative to another complementary electron for certain kinematical conditions. There have been several attempts to parametrize the 5DCS without loss of generality. The goal of such parametrizations is to reduce the

complexity of the 5DCS, which is a real valued function on $R^5$, into functions of a lower dimensionality. A very successful parametrization had been suggested by Huetz *et al* [1] and later by Malegat *et al* [2]. They introduced two complex functions which depend only on the energy of the two electrons and their relative angle $\Theta_{12} = \cos^{-1}(\hat{e}_1 \cdot \hat{e}_2)$. With this parametrization the 5DCS, in the case of linear polarization, separates into geometrical factors and dynamical parameters

$$5DCS = \frac{d^5\sigma}{dE_1\, d\Omega_1\, d\Omega_2} = |a_g(\cos\Theta_1 + \cos\Theta_2) + a_u(\cos\Theta_1 - \cos\Theta_2)|^2, \tag{1}$$

where $\Theta_1$ and $\Theta_2$ are the polar angles of both electrons with respect to the polarization vector. Here $a_g(E_1, E_2, \Theta_{12})$ and $a_u(E_1, E_2, \Theta_{12})$ are complex amplitudes, g and u stand for gerade and ungerade, or symmetric and antisymmetric, with respect to the permutation of $E_1$ and $E_2$: $a_g(E_1, E_2, \Theta_{12}) = a_g(E_2, E_1, \Theta_{12})$ and $a_u(E_1, E_2, \Theta_{12}) = -a_u(E_2, E_1, \Theta_{12})$. The cosine terms in 1 reflect the $^1P^o$ symmetry of the final state. The amplitudes $a_g$ and $a_u$ contain the full three-body dynamics. The advantages of this parametrization are obvious. On the one hand, a data reduction is achieved without losing any information. On the other hand, there is a possibility for a detailed study of the electron dynamics.

Equation (1) can also be written as

$$5DCS = |a_g|^2(\cos\Theta_1 + \cos\Theta_2)^2 + |a_u|^2(\cos\Theta_1 - \cos\Theta_2)^2$$
$$+ 2(\cos^2\Theta_1 - \cos^2\Theta_2)\,\mathrm{Re}\{a_g a_u^*\}. \tag{2}$$

Hence, the full dynamical information of the PDI of helium for linearly polarized light is given by $|a_g|$, $|a_u|$ and $\mathrm{Re}\{a_g a_u^*\} = |a_g||a_u|\cos\zeta$ with $\zeta$ being the relative phase between $a_g$ and $a_u$.

There are three approaches to extract information on the individual functions $|a_g|$, $|a_u|$ and $\mathrm{Re}\{a_g a_u^*\}$ from experimentally measured 5DCSs. The first approach exploits the fact that for equal energy sharing, $E_1 = E_2$, or in the vicinity of threshold, the function $|a_u|$ vanishes and the 5DCS depends solely on $|a_g|^2$ [1, 2].

$$\left.\frac{d^5\sigma}{dE_1\, d\Omega_1\, d\Omega_2}\right|_{E_1=E_2} = |a_g|^2(\cos\Theta_1 + \cos\Theta_2)^2. \tag{3}$$

In this way the function $|a_g(E_1 = E_2)|^2$ measured 20 eV above threshold was found to have essentially Gaussian shape centred at $\Theta_{12} = 180°$ [3]. A Gaussian shape is expected from Wannier's theory for the threshold region of this process [4]. Subsequent experiments between 100 meV and 80 eV above threshold were well described using the Gaussian ansatz [5, 9–12]. The second approach proposed by Krässig [6] makes use of the four experimental configurations where either $(\cos\Theta_1 - \cos\Theta_2)$, $(\cos\Theta_1 + \cos\Theta_2)$, $\cos\Theta_2$, or $\cos\Theta_1$ are zero to extract $|a_g|^2$, $|a_u|^2$ and $\mathrm{Re}\{a_g a_u^*\}$ independent of the energy sharing. The method used in this paper is based on this idea and will be outlined in section 2. The third approach of Bolognesi *et al* [13] utilizes three internormalized data sets measured with the same energy sharing but different geometries to diagonalize a system of three equations with three unknowns $|a_g|^2$, $|a_u|^2$ and $\mathrm{Re}\{a_g a_u^*\}$ for all instances where the three measurements have the value of $\Theta_{12}$ in common. This work reported also near Gaussian shapes for $|a_g|^2$ and $|a_u|^2$ in the case of unequal energy sharing, with $|a_u|^2$ having a narrower width than $|a_g|^2$.

Let us now turn to the parametrization for circularly polarized light. According to Huetz *et al* [1] the 5DCS for left and right circularly polarized light, using $\Phi_{12} = \Phi_2 - \Phi_1$, is

given by

$$5\text{DCS}_{\sigma\pm} = \frac{\mathrm{d}^5\sigma}{\mathrm{d}E_1\,\mathrm{d}\Omega_1\,\mathrm{d}\Omega_2} = \frac{1}{2}\{|a_g(\sin\Theta_1 + \sin\Theta_2\,\mathrm{e}^{\pm i\Phi_{12}}) - a_u(\sin\Theta_1 - \sin\Theta_2\,\mathrm{e}^{\pm i\Phi_{12}})|^2\}$$

(4)

which is equivalent to

$$
\begin{aligned}
5\text{DCS}_{\sigma\pm} = \tfrac{1}{2}\{&|a_g|^2(\sin^2\Theta_1 + \sin^2\Theta_2 + 2\sin\Theta_1\sin\Theta_2\cos\Phi_{12})\\
&+ |a_u|^2(\sin^2\Theta_1 + \sin^2\Theta_2 - 2\sin\Theta_1\sin\Theta_2\cos\Phi_{12})\\
&- 2(\sin^2\Theta_1 - \sin^2\Theta_2)\,\text{Re}\{a_g a_u^*\} \mp 4\sin\Theta_1\sin\Theta_2\sin\Phi_{12}\,\text{Im}\{a_g a_u^*\}\}.
\end{aligned}
$$

(5)

In this case $\Theta_1$ and $\Theta_2$ are the angles of both electrons with respect to the light propagation. While only the real part of $\{a_g a_u^*\}$ is needed for the PDI with linearly polarized light, one also needs the imaginary part of $\{a_g a_u^*\}$ to have the complete information about the three particle breakup in the presence of circularly polarized light.

Equation (5) differs for 5DCS with left and right circularly polarized light just in one sign reversal. Subtracting the 5DCS for right and left circularly polarized light everything but the imaginary term cancels. For $\Theta_1 = \Theta_2 = 90°$ (which means that both electrons are in the plane perpendicular to the light propagation) the difference between $5\text{DCS}_{\sigma^+}$ and $5\text{DCS}_{\sigma^-}$ is identical to the unnormalized circular dichroism (CD):

$$
\begin{aligned}
\text{CD} &\equiv 5\text{DCS}_{\sigma^+} - 5\text{DCS}_{\sigma^-}\\
&= -4\sin(\Phi_{12})\,\text{Im}\{a_g a_u^*\} = -4\sin(\Phi_{12})|a_g||a_u|\sin\zeta.
\end{aligned}
$$

(6)

Occurrence of CD in DPI on He was predicted by Berakdar and Klar in the case when the axial vector of the rotating electric field and the two electron momenta form a left-handed or right-handed tripod [14, 15].

To summarize, for a unique determination of the full phase difference $\zeta$ between the gerade and ungerade amplitudes one needs measurements that provide the sine and cosine of the phase. By using two different COLTRIMS data sets for the PDI of helium with linearly and circularly polarized light (see also parts I and II), a unique value for the phase can be obtained. We have measured the fully differential cross section of the PDI of helium with linearly and circularly (left and right) polarized light at energies $E_{\text{exc}} = 100$ eV and $E_{\text{exc}} = 450$ eV above the threshold at the beamline 4.0.2 [16] of the Advanced Light Source at the Lawrence Berkeley National Laboratory; this paper is a companion paper to two other papers (hereafter called parts I and II). In these two we have presented the angular distributions of the slow and the fast electron for various energy sharings for both linearly (part I) and circularly (part II) polarized light. A complete description of our experimental setup, the analysis and the normalization of the PDI data and a description of the convergent close-coupling (CCC) theory can be found in part I.

The purpose of this paper is to extract the square of the gerade $|a_g|^2$ and ungerade $|a_u|^2$ amplitudes and their relative phase $\zeta$ out of the complete COLTRIMS data set 100 eV and 450 eV above the threshold. We compare our results for $|a_g|^2$, $|a_u|^2$ and the relative phase $\zeta$ with CCC calculations.

## 2. Method of extracting the amplitudes and their relative phase

In this section we will outline the method of determining the functions $|a_g|^2$, $|a_u|^2$ and $\text{Re}\{a_g a_u^*\}$ from a COLTRIMS data set. In the present context this was only done for the experiments with linear polarization, but the technique can be easily modified to be applicable

to arbitrary states of photon polarization. A complete description of the technique will be given elsewhere [7].

Just as taking $E_1 = E_2$ which makes $a_u$ vanish from (1) to derive (3) we are singling out observation angles for which (A) $\cos \Theta_1 = \cos \Theta_2$. We then obtain a result that is proportional to $|a_g|^2$. Similarly, at observation angles for which (B) $\cos \Theta_1 = -\cos \Theta_2$, the result is proportional to $|a_u|^2$. Furthermore, if data for the two cases where $\cos \Theta_i$ of (C) the slow electron and (D) of the fast electron are equal to zero, the difference between those two sets (C − D) is proportional to $|a_g a_u^*| \cos \zeta$.

The electron detection in a COLTRIMS experiment often extends over $4\pi$ solid angle and one can easily sort the full event mode data set into subsets according to the selection criteria (A)–(D). Such subsets are automatically internormalized and, when the sum of all events is recalibrated to the known double ionization cross section, the subsets are also on an absolute cross section scale. One has to keep in mind, though, that in practice one will not require that the relations (A)–(D) be identically zero, but to be smaller than a chosen interval $\Delta$. As a consequence there will be a small contamination from $|a_u|^2$ in case A and from $|a_g|^2$ in case B. However, one can account for this if the exact amounts of contamination are known.

Selecting a subset of COLTRIMS data for double ionization in helium within a width $\Delta$ of one of the event data components is the equivalent of integrating the 5DCS of 1 over the width $\Delta$ in the variable corresponding to this component, and over the entire range of values for the other variables. For any such integration it is useful to revert from the four polar angles of the two electron momenta in the laboratory frame to three Euler angles $\alpha, \beta, \gamma$ which rotate from the laboratory frame to the plane which is spanned by the two momentum vectors [8], plus the interelectron angle $\Theta_{12}$. The conditions on $\cos \Theta_i$ become conditions on the angle $\gamma$. It holds

$$\gamma = \tan^{-1} \left( \frac{(\cos \Theta_1 - \cos \Theta_2)/\sin \frac{\Theta_{12}}{2}}{(\cos \Theta_1 + \cos \Theta_2)/\cos \frac{\Theta_{12}}{2}} \right). \tag{7}$$

Integrating over $\alpha$ and $\beta$ gives a factor of $8\pi/3$ and (1) becomes

$$\frac{d^3 \sigma^{2+}(E_\gamma)}{d\gamma \, d\cos \Theta_{12} \, dE_1} = \frac{1}{\pi} \left( A \cos^2 \gamma + B \sin^2 \gamma + (C - D) \frac{\sin 2\gamma}{2} \right), \tag{8}$$

where the roman letters A, B, C, D were used as abbreviations for

$$A := \frac{16\pi^2}{3} |a_g|^2 (1 + \cos \Theta_{12}),$$

$$B := \frac{16\pi^2}{3} |a_u|^2 (1 - \cos \Theta_{12}), \tag{9}$$

$$C - D := \frac{32\pi^2}{3} |a_g a_u^*| \cos \zeta \sin \Theta_{12}.$$

From (8) it is seen that for $\gamma = 0$ or $\gamma = \pi$ only the term proportional to $|a_g|^2$ remains, $\gamma = \pi \pm \pi/2$ singles out the term with $|a_u|^2$ and the difference of the two cases with $\gamma = \pm\pi/4$ or $\gamma = \pi \pm \pi/4$ leaves the cross term. It can also be seen that any deviation from those $\gamma$ values will give admixtures from the other terms. By integrating (8) over the width $\pm\Delta$ around these particular $\gamma$ values we determine the exact amounts of admixture for each term. We choose $\Delta = \pi/4$ and make use of the entire $2\pi$ range in $\gamma$, and thus of the entire data set, for the determination of $|a_g|^2$, $|a_u|^2$ and $|a_g a_u^*| \cos \zeta$. We use script letters $\mathscr{A}, \mathscr{B}, \mathscr{C}, \mathscr{D}$ for the integrals of the differential cross section (8) over those regions in $\gamma$,

$$\mathscr{A} = \int_{\{\mathscr{A}\}} \frac{d^3 \sigma^{2+}}{\cdots} \, d\gamma = \frac{1}{2} \left( \left( 1 + \frac{2}{\pi} \right) A + \left( 1 - \frac{2}{\pi} \right) B \right), \tag{10}$$

$$\mathscr{B} = \int_{\{\mathscr{B}\}} \frac{d^3\sigma^{2+}}{\cdots} d\gamma = \frac{1}{2}\left(\left(1 + \frac{2}{\pi}\right)B + \left(1 - \frac{2}{\pi}\right)A\right), \tag{11}$$

$$\mathscr{C} - \mathscr{D} = \int_{\{\mathscr{C}\}} \frac{d^3\sigma^{2+}}{\cdots} d\gamma - \int_{\{\mathscr{D}\}} \frac{d^3\sigma^{2+}}{\cdots} d\gamma = \frac{2}{\pi}(C - D), \tag{12}$$

with

$$\{\mathscr{A}\} = \left[-\frac{\pi}{4}, \frac{\pi}{4}\right), \left[\frac{3\pi}{4}, \frac{5\pi}{4}\right), \qquad \{\mathscr{B}\} = \left[\frac{\pi}{4}, \frac{3\pi}{4}\right), \left[\frac{5\pi}{4}, \frac{7\pi}{4}\right),$$

$$\{\mathscr{C}\} = \left[0, \frac{\pi}{2}\right), \left[\pi, \frac{3\pi}{2}\right), \qquad \{\mathscr{D}\} = \left[\frac{\pi}{2}, \pi\right), \left[\frac{3\pi}{2}, 2\pi\right).$$

The admixtures to A and B are easily removed with the transformations

$$A = \frac{\pi + 2}{4}\mathscr{A} - \frac{\pi - 2}{4}\mathscr{B}; \qquad B = \frac{\pi + 2}{4}\mathscr{B} - \frac{\pi - 2}{4}\mathscr{A}.$$

The $\Theta_{12}$-dependent weight factors in (9) are the reason for poor counting statistics in $|a_g|^2$ near $\Theta_{12} = \pi$, in $|a_u|^2$ near $\Theta_{12} = 0$, and in $|a_g a_u^*|\cos\zeta$ near $\Theta_{12} = 0$ and $\pi$.

In this work we obtained the sine of the relative phase $\zeta$ from the measurement of the circular dichroism according to (6). In that measurement we made use of the fact that the 5DCS for circular polarization has rotational symmetry about the direction of incident radiation. In the same way for linear polarization there is rotational symmetry about the polarization direction. This means that the 5DCS only depends on the difference of azimuthal angles $\Phi_{12} = \Phi_1 - \Phi_2$. In a COLTRIMS data set we can therefore sort according to $\Phi_{12}$ irrespective of the individual values and improve the counting statistics. The result is equivalent to the fourfold differential cross section 4DCS $= 2\pi$ 5DCS.

## 3. Results

The experimental results are divided into two parts. First $|a_g|^2$, $|a_u|^2$, their ratio and the phase $\zeta$ will be shown for $E_{exc} = 100$ eV, followed by the results for $E_{exc} = 450$ eV and a comparison between the two. In the companion papers parts I and II it was already established that our differential cross section data are well reproduced by CCC calculations. Here we will compare experiment and theory on the level of $|a_g|^2$, $|a_u|^2$ and the phase $\zeta$. The solid line in all figures is the velocity form of the CCC calculation. The length and acceleration forms yield results indistinguishable from the velocity form and are hence not presented.

### 3.1. 100 eV

In figures 1–4 we present the four parameters characterizing $a_g$ and $a_u$ for five energy sharings at 100 eV above the threshold. Figures 1 and 2 show $|a_g|^2$ and $|a_u|^2$, respectively. We chose the same energy sharings as we did in parts I and II: 1.5 eV $\leftrightarrow$ 98.5 eV; 10 eV $\leftrightarrow$ 90 eV; 20 eV $\leftrightarrow$ 80 eV; 30 eV $\leftrightarrow$ 70 eV and 50 eV $\leftrightarrow$ 50 eV.

The maximum value of $|a_g|^2$ for all energy sharings can be found for antiparallel emission. At equal energy sharing, figure 1(e), our data are consistent with the selection rule that the cross section is zero for emission of two electrons with the same energies into the same direction ($\Theta_{12} = 0°$). Figure 1(a) shows that this selection rule does not apply for unequal energy sharing; the velocity difference between both electrons is large enough that they can be emitted into the same direction. This can also be seen in the angular distributions for linearly polarized light in the condition for extreme unequal energy sharing (part I, figures 6(a)+(i)).
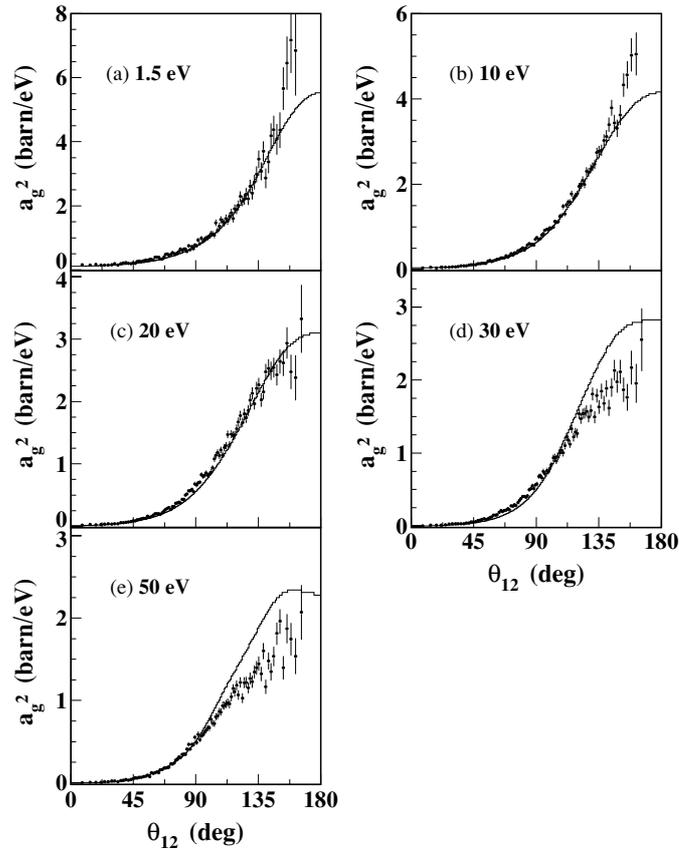
**Figure 1.** $|a_g|^2$ at $E_{exc} = 100$ eV on absolute scale. The whole COLTRIMS data set for linearly polarized light is used for extracting $|a_g|^2$. The solid line is the velocity form of a CCC calculation. Energy integration of one of both electrons: (a) $0 < E_e < 3$ eV, (b) $5 < E_e < 15$ eV, (c) $15 < E_e < 25$ eV, (d) $25 < E_e < 35$ eV, (e) $45 < E_e < 55$ eV.

In an angular distribution plot for linearly polarized light the contribution of parallel emission is given solely by $|a_g|^2$:

$$4DCS(E_1, \Theta_{12} = 0°) = 8\pi |a_g(E_1, \Theta_1, \Theta_{12} = 0°)|^2 \cos^2 \Theta_1. \tag{13}$$

Comparing our results with the velocity form of the CCC calculation we find generally good agreement. In the peak region experiment is higher than theory in the cases of very asymmetric energy sharing, and experiment is lower than theory for the less asymmetric energy sharings. In the equal energy sharing case theory predicts the maximum of $|a_g|^2$ to be at $\Theta_{12} \approx 150°$.

It is interesting that all the $|a_g|^2$ are approximately Gaussian shaped as in the Wannier prediction for the threshold region. This feature must have a broader range of applicability than other predictions from that theory. For example, Knapp *et al* [17] have found that the breakup of the electron pair at 100 eV excess energy is preferentially parallel to the polarization axis in contrast to the Wannier prediction of perpendicular emission.

The shapes of $|a_u|^2$ in figure 2 show a greater variation with the energy sharing. For unequal energy sharing the functions $|a_u|^2$ also have their maximum at $\Theta_{12} = 180°$ and in the vicinity of the maximum the functions are bell shaped, with a width that is narrower than for
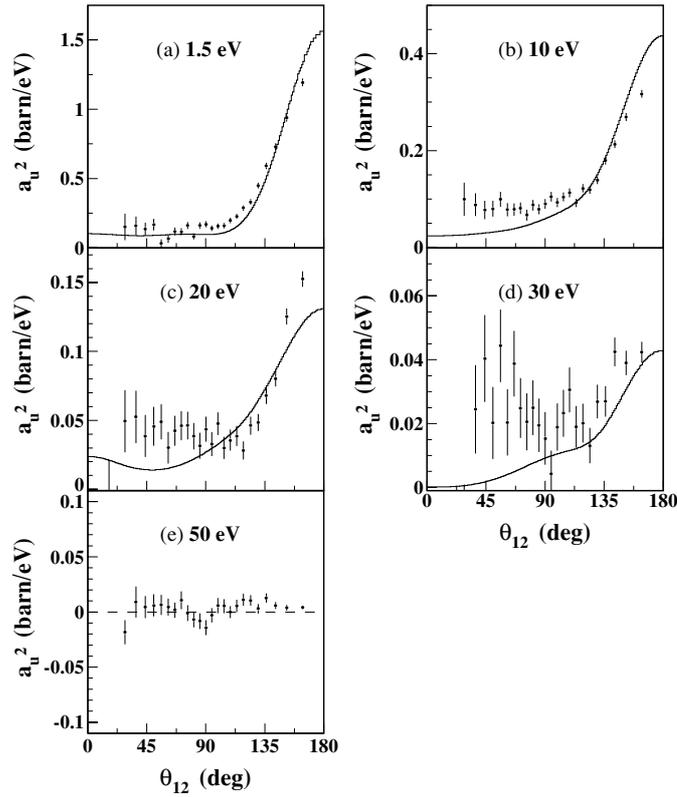
**Figure 2.** $|a_u|^2$ at $E_{exc} = 100$ eV on absolute scale. The solid line is the velocity form of a CCC calculation. Energy integration of one of both electrons: (a) $0 < E_e < 3$ eV, (b) $5 < E_e < 15$ eV, (c) $15 < E_e < 25$ eV, (d) $25 < E_e < 35$ eV, (e) $45 < E_e < 55$ eV. To guide the eye, a dashed line is drawn at $|a_u|^2 = 0$ in panel (e).

$|a_g|^2$ cases. Also, for smaller values of $\Theta_{12}$ the $|a_u|^2$ functions approach a near constant level. For equal energy sharing the experimental amplitude $|a_u|^2$ is consistent with the expected zero within the error bars, which serves as a good consistency check of our data.

Figure 3 shows the ratio between $|a_g|^2$ and $|a_u|^2$. For all energy sharings the maxima of $|a_g|^2$ are higher than $|a_u|^2$. The maximum value of the ratio decreases with increasing asymmetry of the energy sharing.

Figure 4 shows the phase $\zeta$ between the two amplitudes. Overall the phase $\zeta$ does not change much for the different energy sharings. There is a trend that the phase $\zeta$ for small $\Theta_{12}$ is higher than for large $\Theta_{12}$. In the region $\Theta_{12} > 90°$ the result of the CCC calculation agrees very well with the experimental data. Below this angle there are discrepancies and the CCC predictions show a very strong variation with energy sharing that is not observed in the experiment. Different CCC calculations show some instability for $\Theta_{12} < 20°$. However, the general downward trend below $\theta_{12} < 90°$ is reproduced consistently.

### 3.2. 450 eV

Figures 5–8 show the shape of $|a_g|^2$, $|a_u|^2$, the ratio $|a_g|^2/|a_u|^2$ and the phase $\zeta$ for different energy sharings at $E_{exc} = 450$ eV. The following energy sharings are chosen: 1.5 eV $\leftrightarrow$ 448.5 eV; 10 eV $\leftrightarrow$ 440 eV; 30 eV $\leftrightarrow$ 420 eV and 50 eV $\leftrightarrow$ 400 eV.
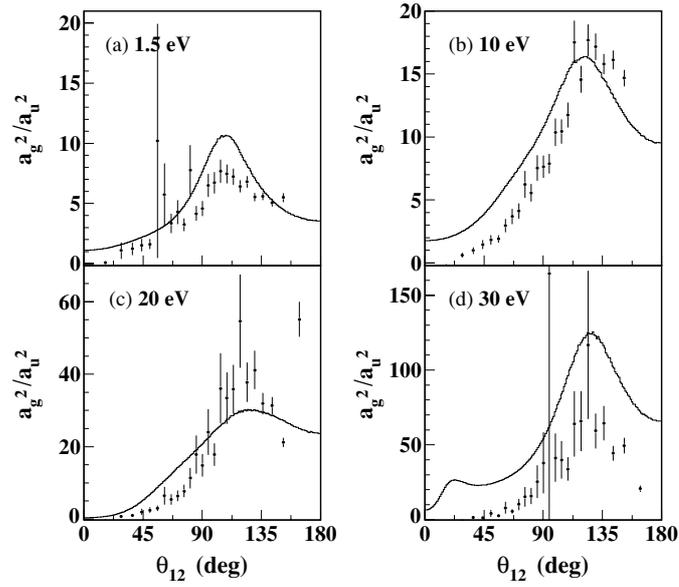
**Figure 3.** $|a_g|^2/|a_u|^2$ at $E_{exc} = 100$ eV. The solid line is the velocity form of a CCC calculation. Energy integration of one of both electrons: (a) $0 < E_e < 3$ eV, (b) $5 < E_e < 15$ eV, (c) $15 < E_e < 25$ eV, (d) $25 < E_e < 35$ eV, (e) $45 < E_e < 55$ eV.
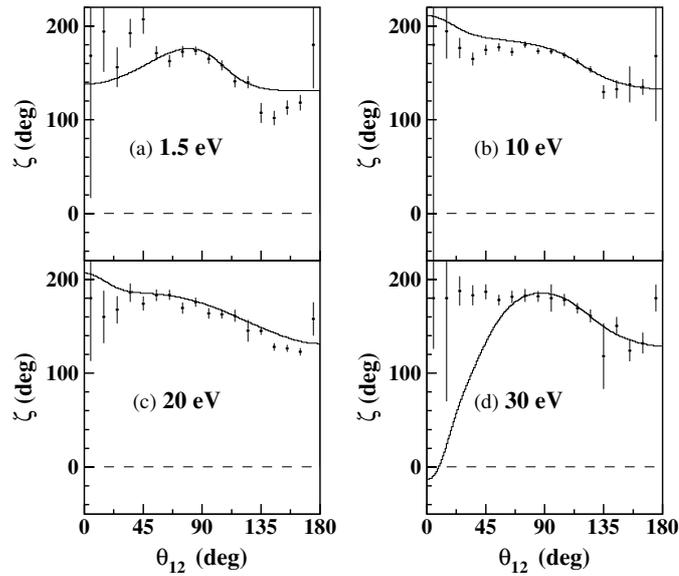


**Figure 4.** Phase between $a_g$ and $a_u$ at $E_{exc} = 100$ eV. The whole COLTRIMS data set for linearly and circularly polarized light is used. The phase $\zeta$ is given by $\sin \zeta = CD/(-4 \sin \Phi_{12} |a_g||a_u|)$. The solid line is the velocity form of a CCC calculation. Energy integration of one of both electrons for linearly and circularly polarized light: (a) $0 < E_e < 3$ eV, (b) $5 < E_e < 15$ eV, (c) $15 < E_e < 25$ eV, (d) $25 < E_e < 35$ eV, (e) $45 < E_e < 55$ eV. For circularly polarized light, the two electrons are in a plane perpendicular to the light propagation: $\Theta_1 = \Theta_2 = 90° \pm 7°$. To guide the eye a dashed line is drawn at $\zeta = 0°$.
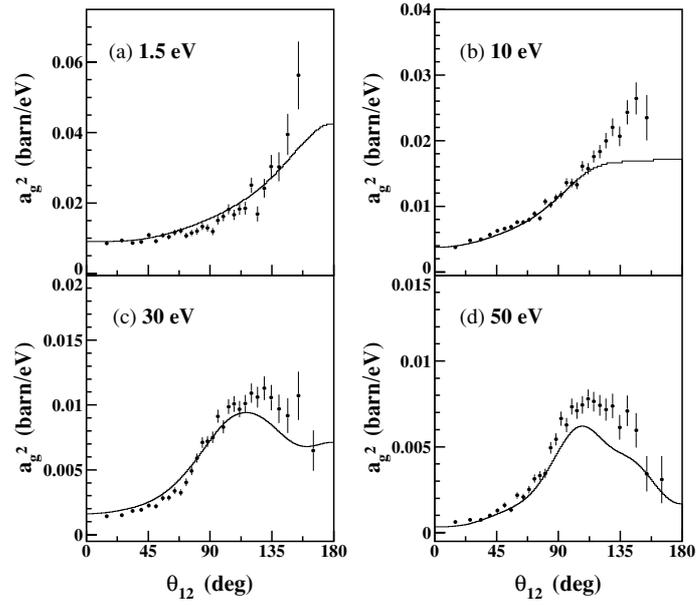
**Figure 5.** $|a_g|^2$ at $E_{exc} = 450$ eV. The data set is normalized to the CCC calculation. The whole COLTRIMS data set for linearly polarized light is used for extracting $|a_g|^2$. The solid line is the velocity form of a CCC calculation. Energy integration of one of both electrons: (a) $0 < E_e < 3$ eV, (b) $5 < E_e < 15$ eV, (c) $25 < E_e < 35$ eV, (d) $45 < E_e < 55$ eV.
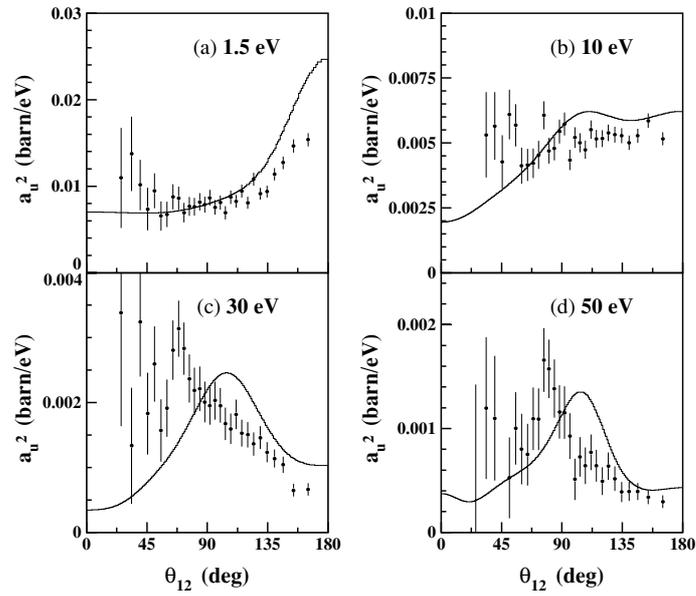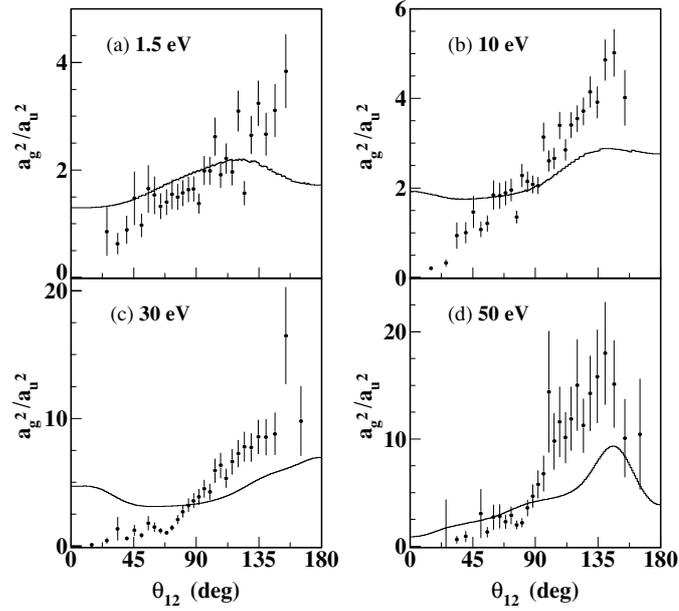


**Figure 6.** $|a_u|^2$ at $E_{exc} = 450$ eV. The data set is normalized to the CCC calculation. The whole COLTRIMS data set for linearly polarized light is used for extracting $|a_u|^2$. The solid line is the velocity form of a CCC calculation. Energy integration of one of both electrons: (a) $0 < E_e < 3$ eV, (b) $5 < E_e < 15$ eV, (c) $25 < E_e < 35$ eV, (d) $45 < E_e < 55$ eV.

**Figure 7.** $|a_{\mathrm{g}}|^2/|a_{\mathrm{u}}|^2$ at $E_{\mathrm{exc}} = 450$ eV. The solid line is the velocity form of a CCC calculation. Energy integration of one of both electrons: (a) $0 < E_e < 3$ eV, (b) $5 < E_e < 15$ eV, (c) $25 < E_e < 35$ eV, (d) $45 < E_e < 55$ eV.
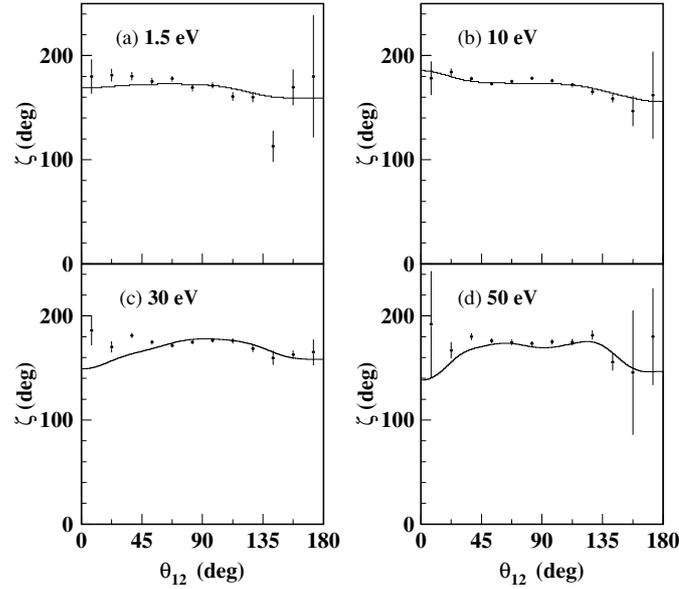


**Figure 8.** Phase between $|a_{\mathrm{g}}|$ and $|a_{\mathrm{u}}|$ at $E_{\mathrm{exc}} = 450$ eV. The whole COLTRIMS data set for linearly and circularly polarized light is used. The phase $\zeta$ is given by $\sin \zeta = \mathrm{CD}/(-4 \sin \Phi_{12} |a_{\mathrm{g}}||a_{\mathrm{u}}|)$. The solid line is the velocity form of a CCC calculation. Energy integration of one of both electrons for linearly and circularly polarized light: (a) $0 < E_e < 3$ eV, (b) $5 < E_e < 15$ eV, (c) $25 < E_e < 35$ eV, (d) $45 < E_e < 55$ eV. For circularly polarized light, the two electrons are in a plane perpendicular to the light propagation: $\Theta_1 = \Theta_2 = 90° \pm 25°$.

Comparing figure 5 and figure 1 shows a strong dependence of $|a_\mathrm{g}|^2$ on the excess energy. Even more striking is the dramatic change of the shape of $|a_\mathrm{g}|^2$ with the energy sharing which signifies a change in the dynamics of the two-electron escape. At extreme unequal energy sharings (figures 5(a) and (b)) we find the amplitude $|a_\mathrm{g}|^2$ to be peaked at $180°$ with a near-Gaussian profile with a constant offset and considerable intensity at $\Theta_{12} = 180°$. At an energy sharing of 30 eV $\leftrightarrow$ 420 eV and 50 eV $\leftrightarrow$ 400 eV (figures 5(c) and (d)), which are still very asymmetric energy sharing, the shape of $|a_\mathrm{g}|^2$ is far from Gaussian, there is no maximum for back-to-back emission. Instead, we find a maximum at $\Theta_{12} \cong 110°$ both in experiment and theory. A hint of a flattening of the amplitude $|a_\mathrm{g}|^2$ and a dip at $\Theta_{12} = 180°$ are seen in the CCC calculations for near symmetric energy sharing cases at 100 eV excess energy, figure 1. This is completely different from all observations at lower excess energies, where the maximum of $|a_\mathrm{g}|^2$ at $\Theta_{12} = 180°$ has always been viewed as the effect of the long-range Coulomb repulsion of the two electrons in the final state. The results in figures 5(c)+(d) show that at high excess energies the dynamical effects cannot be characterized simply on the basis of the electron–electron repulsion in the final state. It seems also clear that these different findings are not caused by a new mechanism because they are reproducible with the same theoretical approach and using the same ingredients as in the cases with lower excess energies.

For $|a_\mathrm{u}|^2$ we find a maximum in the experiment for $\Theta_{12} = 180°$ only in the case of the most extreme energy sharing, figure 6(a), and it comes with a significant offset. Already at an energy sharing of 10 eV $\leftrightarrow$ 440 eV, figure 6(b), the experimental data of this function could be described as almost constant. The cases in figures 6(c) and (d) are yet different, with a narrow maximum at $\Theta_{12} \approx 70°$ and very small values near $\Theta_{12} = 180°$. The CCC calculations reproduce the general trend in the data, but differ in some aspects, e.g., in the position of the maxima in figure 6(c) and (d). We note that for an energy sharing of 30 eV $\leftrightarrow$ 420 eV, $|a_\mathrm{g}|^2$ for $\Theta_{12} = 0°$ (figure 5(c)) is higher than $|a_\mathrm{u}|^2$ for $\Theta_{12} = 180°$ (figure 6(c)). While the 5DCS for parallel emission is obtained by $4|a_\mathrm{g}(E_1, E_2, \Theta_{12} = 0°)|^2$ (equation (13)), the 5DCS for antiparallel emission can be expressed by $4|a_\mathrm{u}(E_1, E_2, \Theta_{12} = 180°)|^2$. This is the reason, why figure 9 of part I shows a larger lobe for parallel rather than for antiparallel emission.

Figure 7 shows the ratio $|a_\mathrm{g}|^2/|a_\mathrm{u}|^2$; this should be compared to figure 3. We find that $|a_\mathrm{u}|^2$ is more prominent in relation to $|a_\mathrm{g}|^2$ at 450 eV than at 100 eV above threshold. Again, the maxima of the ratio decreases with increasing asymmetry of the energy sharing.

Figure 8 shows the phase $\zeta$. The phase is almost independent of $\Theta_{12}$ (flat curve) and almost independent of the energy sharing.

We attribute the change in shape of $|a_\mathrm{g}|^2$ and $|a_\mathrm{u}|^2$ with energy sharing to the interplay between the two different ionization mechanisms, the shake-off as a result of the relaxation of the ionic potential, and knock-out [21] by collision of the electron that absorbed the photon with the other electron [18]. These mechanisms seem to be active at different energy sharings. Knapp *et al* [19] argued that, at an extreme asymmetric energy sharing, an observed value of the anisotropy parameter $\beta \simeq 2$ for the fast electron makes it possible to distinguish the two electrons as 'primary' and as 'secondary' electrons. While the primary electron absorbs energy and angular momentum of the photon, the secondary electron is either shaken-off or knocked out. The angular distributions show clearly a dominance of the shake-off for extreme unequal energy sharing. However, to be promoted to the continuum with 30 eV or more, it appears that the slow electron needs a hard binary collision.

The connection of the shake-off and knock-out mechanisms with the shape of the amplitudes is straightforward. A mostly isotropic shape with a slightly backward emission is expected for the shake-off mechanism [20]. This is exactly what the shape of $|a_\mathrm{g}|^2$ and $|a_\mathrm{u}|^2$

reveals for 1.5 eV $\leftrightarrow$ 448.5 eV: a more or less isotropic distribution (note a high constant offset in figures 5(a) and 6(a) comparing to figures 1(a) and 2(a)) with a slightly backward emission can be found in figures 5(a) and 6(a). At an energy of 10 eV $\leftrightarrow$ 440 eV a cross-over between the two mechanisms occurs. At an energy sharing of 30 eV $\leftrightarrow$ 420 eV and 50 eV $\leftrightarrow$ 400 eV the peak in $|a_g|^2$ and $|a_u|^2$ around $\Theta_{12} \cong 110°$ is due to knock-out, which is a binary collision between particles of equal mass, hence one expects it to peak *classically* at $\Theta_{12} = 90°$. We note that a slight shift of the maximum of $|a_g|$ away from 180° at $E_1 = E_2 = 50$ eV (figure 1) might be a hint of the same—not quite as hard—binary collision.

In summary, we have presented a method of extracting $|a_g|^2$, $|a_u|^2$ and the phase $\zeta$ for a COLTRIMS data set. We have presented $|a_g|^2$, $|a_u|^2$ and the phase $\zeta$ for an energy 100 eV and 450 eV above threshold. The $|a_g|^2$ and $|a_u|^2$ have a Gaussian shape at 100 eV above threshold. The width of $|a_u|^2$ is smaller than that of $|a_g|^2$. There is only a weak dependence of the phase on energy sharing. For 450 eV above threshold a dramatic change of the dynamical parameters with energy sharing is observed. For extreme asymmetric energy sharing $|a_g|^2$ and $|a_u|^2$ show a high offset: while at higher energies for the slow electron $|a_g|^2$ and $|a_u|^2$ have a peak at $\Theta_{12} \cong 110°$. This provides direct evidence for the shake-off ionization mechanism dominating at extremely asymmetric energy sharing, and knock-out contributing to the cases where the slow electron has 30 eV or more kinetic energy.

## Acknowledgments

## References

[1] Huetz A, Selles P, Waymel D and Mazeau J 1991 *J. Phys. B: At. Mol. Opt. Phys.* **24** 1917
[2] Malegat L, Selles P and Huetz A 1997 *J. Phys. B: At. Mol. Opt. Phys.* **30** 251
[3] Schwarzkopf O, Krässig B, Elmiger J and Schmidt V 1993 *Phys. Rev. Lett.* **70** 3008
[4] Rau A R P 1976 *J. Phys. B: At. Mol. Phys.* **9** L283
[5] Huetz A and Mazeau J 2000 *Phys. Rev. Lett.* **85** 530
[6] Krässig B 2002 *Proc. Int. Symp. on (e,2e), Double Photoionization and Related Topics (AIP Conference Proc.)* vol 604 p 12
[7] Krässig B in preparation
[8] Nikitin S I and Ostrovsky V N 1985 *J. Phys. B: At. Mol. Phys.* **18** 4349 (note the misprint in equation (2.16))
Bogdanovich *et al* 1997 *J. Phys. B: At. Mol. Opt. Phys.* **30** 921
[9] Schwarzkopf O and Schmidt V 1995 *J. Phys. B: At. Mol. Opt. Phys.* **28** 2847
[10] Dawber G, Avaldi L, McConkey A G, Rojas H, MacDonald M A and King G C 1995 *J. Phys.* **28** L271
[11] Turri G, Avaldi L, Bolognesi P, Camilloni R, Coreno M, Berakdar J, Kheifets A S and Stefani G 2002 *Phys. Rev.* A **65** 034702
[12] Dörner R *et al* 1998 *Phys. Rev.* A **57** 1074
[13] Bolognesi P, Kheifets A S, Bray I, Malegat L, Selles P, Kazansky A K and Avaldi L 2003 *J. Phys. B: At. Mol. Opt. Phys.* **36** L241
[14] Berakdar J and Klar H 1992 *Phys. Rev. Lett.* **69** 1175

[15] Berakdar J, Klar H, Huetz A and Selles P 1993 *J. Phys. B: At. Mol. Opt. Phys.* **26** 1463
[16] Young A T *et al* 2001 *Nucl. Instrum. Methods* A **549** 467
[17] Knapp A *et al* 2002 *J. Phys. B: At. Mol. Opt. Phys.* **35** L521
[18] Samson J A R 1990 *Phys. Rev. Lett.* **65** 2861
[19] Knapp A *et al* 2002 *Phys. Rev. Lett.* **89** 033004
[20] Shi T Y and Lin C D 2002 *Phys. Rev. Lett.* **89** 163202
[21] Schneider T, Chocian P L and Rost J-M 2002 *Phys. Rev. Lett.* **89** 073002